

Article

Optimization of the Uniformity Index Performance in the Selective Catalytic Reduction System Using a Metamodel

Sunghun Kim ¹, Youngjin Park ¹, Seungbeom Yoo ¹, Sejun Lee ², Uttam Kumar Chanda ², Wonjun Cho ³ and Ocktaeck Lim ^{4,*}

¹ Sejong R&D Center, 23 Hyosan 1-gil, Buk-gu, Ulsan 44252, Republic of Korea; windy0707@sjku.co.kr (S.K.); pyj031388@sjku.co.kr (Y.P.); sbyoo@sjku.co.kr (S.Y.)

² Research Center for Next Generation Vessel with Hydrogen Fuel Cell, University of Ulsan, San 29, Mugeo2-dong, Nam-gu, Ulsan 44610, Republic of Korea; ggryor@ulsan.ac.kr (S.L.); uttam031@ulsan.ac.kr (U.K.C.)

³ BIO FRIENDS Inc., HQ 514, 199, Techno2 Street, Yuseong District, Daejeon 34025, Republic of Korea; williamcho86@bfi.co.kr

⁴ School of Mechanical Engineering, University of Ulsan, San 29, Mugeo2-dong, Nam-gu, Ulsan 44610, Republic of Korea

* Correspondence: otlim@ulsan.ac.kr; Tel.: +82-10-7151-8218

Abstract: The significance of the selective catalytic reduction system in vehicles increases in line with the high standards of emission control and enhanced selective catalytic reduction efficiency. This study aims to improve the performance of the selective catalytic reduction system through an optimization method using a metamodel. The objective function is defined as the ammonia uniformity index, and the design parameters are defined in relation to the pipe length and mixer related to the chemical reaction of the urea solution. The range of design parameters has been designated by a trial-and-error method in order to maintain the overall design drawings of the selective catalytic reduction system and prevent modeling errors. Three algorithms, namely, ensemble decision tree, Kriging, and radial basis function, are employed to develop the metamodel. The accuracy of the metamodel is verified based on three indicators: the normalized root mean square error, root mean square error, and maximum absolute error. The metamodel is generated using the Kriging model, which has the highest accuracy among the algorithms, and optimization is also performed. The predicted optimization results are confirmed by computational fluid dynamics numerical analysis with a 99.83% match. The ammonia uniformity index is improved by 1.38% compared to the base model, and it can be said that the NO_x purification efficiency is improved by 30.95%. Consequently, optimizing the uniformity index performance through structural optimization is of utmost importance. Furthermore, this study reveals that the design variables related to the mixer play a crucial role in the performance. Therefore, using the metamodel to optimize the selectively catalytic reduction system's structure should be considered significant. Finally, in the future, the analysis model can be validated using test equipment based on the findings of this study.

Keywords: selective catalytic reduction; design of experiments; optimal design; sequential sampling; metamodel



Citation: Kim, S.; Park, Y.; Yoo, S.; Lee, S.; Chanda, U.K.; Cho, W.; Lim, O. Optimization of the Uniformity Index Performance in the Selective Catalytic Reduction System Using a Metamodel. *Sustainability* **2023**, *15*, 13803. <https://doi.org/10.3390/su151813803>

Academic Editor: Matthew Jones

Received: 3 July 2023

Revised: 7 August 2023

Accepted: 24 August 2023

Published: 15 September 2023



Copyright: © 2023 by the authors. Licensee MDPI, Basel, Switzerland. This article is an open access article distributed under the terms and conditions of the Creative Commons Attribution (CC BY) license (<https://creativecommons.org/licenses/by/4.0/>).

1. Introduction

Environmental problems are global issues, resulting in the tightening of the emission standards of internal combustion engines. In particular, diesel vehicles have the advantages of better fuel economy and higher engine power and torque than gasoline vehicles of the same engine displacement, but they emit major pollutants such as hydrocarbons (HCs), nitrogen oxide (NO_x), carbon monoxide (CO), and particulate matter (PM). These pollutants are strictly regulated worldwide [1]. To satisfy these strict regulations, research is being conducted to improve the performance of after-treatment devices/systems such as diesel

particulate filters (DPFs), selective catalytic reduction (SCR), and exhaust recirculation (EGR) [2]. Diesel vehicles use selective catalytic reduction (SCR), which is regarded as one of the best technologies for meeting strict NO_x reduction requirements [3]. The uniformity index (UI) of ammonia is suitable for evaluating the SCR performance in a system because of its contribution to the NO_x conversion efficiency and increase in the catalyst life [4]. Many factors should be considered before designing the SCR system [5,6]. In the SCR system, either the low density of NH₃ in the exhaust gas degrades the conversion efficiency of NO_x or the catalyst is damaged by the excessive density of NH₃ [7]. Furthermore, there are many studies to improve UI performance. When the injection angle of ammonia is arranged in the direction of the exhaust gas flow, it improves the UI performance by 16% from the initial model [8]. The mixer equipped in the exhaust pipe causes a vortex that not only performs effective mixing of the exhaust gas and ammonia but also delays wall wetting, making a vigorous hydrolysis and thermolysis environment. As a result, it attains a 17.95% improvement in UI performance from the initial model [9]. Ye et al. [10] developed a three-dimensional simulation model to investigate the NH₃ uniformity and conversion rate produced by the urea–water solution spray system. The results showed that the impact of the mixer is significant, and the use of a dual-mixer results in a remarkable increase in the urea conversion rate and NH₃ uniformity index by 169.5% and 136.4%, respectively. The techniques mentioned above are optimized using methods of trial-and-error and the design of experiment (DOE) [11,12]. These methods can help in easily planning experiments; however, it is difficult to represent the performance across the entire range of the design. It is also difficult to analyze the interrelationship between different design parameters. Therefore, there is a need for a systematic optimization method, and recent studies related to optimization using a metamodel can be considered.

The metamodel consists of algorithms that are ensemble decision tree (EDT), Kriging, and radial basis function (RBF). Identifying the characteristics of the data is extremely complex, and it is difficult to consider the most suitable optimization algorithm. It is important to select appropriate algorithms according to the characteristics of the data such as nonlinearity [13,14]. Hoang et al. [12] studied seismic fragility analysis using the Kriging metamodel of concrete highway bridges. The generated metamodel was evaluated for accuracy using a cross-validation method. Three major predictive indicators of errors such as root mean square error, R^2 , and relative maximum absolute error (RMAE) have been used in this study. Several researchers have described that the time required for the numerical analysis may be reduced by the application of sequential sampling, wherein the number of samples is minimized [15,16]. Woo et al. [17] performed a contribution analysis to identify the design parameters that are effective in improving performance. The concept of a high-performance car chassis is developed using virtual prototyping and optimized to ensure consistency in the performance predictions. Recently, the optimization of the shape of a permanent magnet synchronous motor (PMSM) was analyzed using a metamodel with Kriging and MLP algorithms. The results showed an improvement not only in torque performance enhancement from the Kriging model by 1.3% and the MLP model by 2.2% but also in the back electromotive force (EMF) by 4.3% [18]. Using the OASIS (Optimization Assisted Simulation Integration Software V1.3) optimization tool, the power of impulse turbines was enhanced by 5.33%, and the analysis cost was reduced [19]. In another work, metamodels were generated by various algorithms, and the best predictive performance results were proposed using Process Integration Automation and Optimization (PIAnO 2023) software (PIDOTEC Inc., Seoul, Republic of Korea) by PIDOTEC Inc. [20]. Different optimization cases have already been studied using PIAnO 2023 software. The optimization of the structural design of a mooring system using PIAnO 2023 software helped in the reduction in cost by more than 52% [21]. The structural optimization of wound-field synchronous machines (WFSMs) using PIAnO 2023 software has also been analyzed [22]. The results showed a significant improvement in torque by 31.66% and a reduction in the torque ripple.

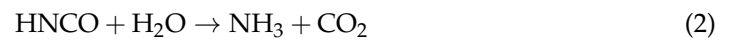
In the present work, the performance of the SCR system is predicted using an optimization technique based on a metamodel. In addition, the procedure of optimization is analyzed and compared with our previous study based on DOE [23]. This study will help in understanding the design factors that significantly affect the optimization of uniformity index performance and thereby improvement in NO_x emission reduction.

2. Methodology

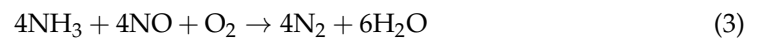
2.1. SCR System and Numerical Analysis

The purpose of the SCR system is to reduce the NO_x of exhaust gas. When the urea solution is injected into the high-temperature exhaust gas, NH₃ is generated through a thermal-decomposition chemical reaction and hydrolysis reaction as shown in Equations (1) and (2), respectively. When it is mixed with exhaust gas and distributed across the catalyst, the NO_x is reduced to nitrogen and water as represented in Equation (3) [24,25].

In the exhaust pipe:



In the SCR catalyst:



NH₃ can be produced sufficiently when the reactions in Equations (1) and (2) are properly activated, which results in the activation of the reaction in Equation (3) in the SCR catalyst [26,27]. Therefore, it is necessary to secure enough space for the initiation of the chemical reaction before NH₃ mixes with the SCR catalyst. Adequate mixing using the mixer should be applied to create a vortex so that the number of sprayed elements can be decomposed properly [28,29] and also the sufficient vaporization of urea solution must be improved [30,31]. For this reason, the SCR system is designed as shown in Figure 1, and each name of the design parameters is mentioned in Table 1. The urea solution is injected from the injector and mixes well with the exhaust as it passes through the mixer due to the vortex. The pressure drop at the SCR cone delays the gas flow and helps to increase flow uniformity. The mixer's performance varies depending on the number of blades configured and the angle of bending. The design parameters mentioned in Table 1 are A (the distance between the injector and mixer), B (the angle at which the exhaust gas meets the urea solution injected by the injector), C (the angle of the injector and mixer), D (the mounting angle of the mixer), E (the number of mixer blades), F (the bending angle of mixer blades), G (the distance between the mixer and SCR cone), and H (the length of the SCR cone).

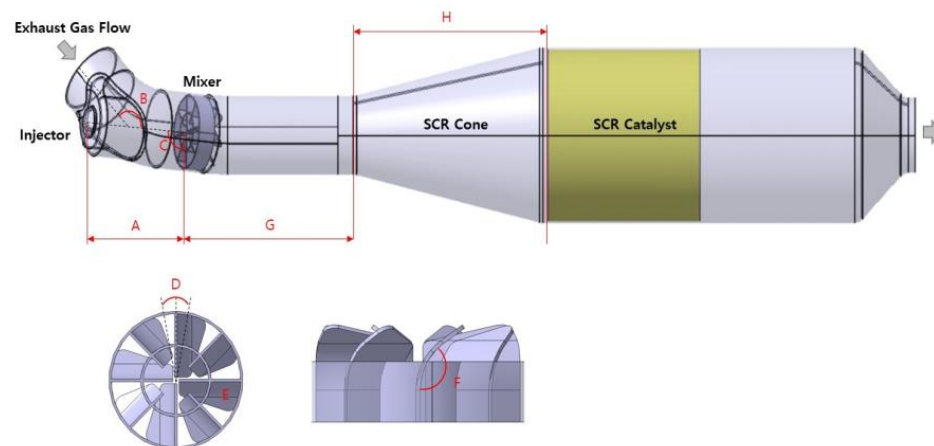


Figure 1. Design of the SCR system.

Table 1. Design parameters of the SCR system.

| No. | Major Design Parameters | Unit |
|-----|---|------|
| 1 | A: Distance between the Urea Injector and Mixer | mm |
| 2 | B: Inflow Angle of the Exhaust Gas | deg. |
| 3 | C: Angle of the Urea Injector and Mixer | deg. |
| 4 | D: Mounting Angle of the Mixer | deg. |
| 5 | E: Number of Mixer Blades | No. |
| 6 | F: Bending Angle of Mixer Blades | deg. |
| 7 | G: Distance between the Mixer and SCR Cone | mm |
| 8 | H: Length of the SCR Cone | mm |

The numerical analysis is calculated using SIEMENS STAR-CCM+, and the boundary conditions are set based on the experimental values. In the previous study [23] and Appendix A (Table A6), the boundary conditions for the numerical analysis are mentioned in detail. Engine conditions are based on the engine running criteria in accordance with EOP5 (Engine Operating Point). The engine speed is 3000 RPM, the exhaust gas mass flow rate is 316 kg/h, the exhaust gas inlet temperature is 411 °C, the urea injection amount is 30.6 mg/injection, the urea injection period is 81.6 ms/Hz, and the exhaust gas outlet pressure is set at 9.8 kPa. Catalysts are implemented using the characteristics of the porous catalyst model wherein the catalyst carrier has a capacity of 3.0 L and a cell density of 600 cpsi. Conditions such as the spray angle, injection pressure, and nozzle diameter of the urea injector are based on a commercial urea injector three-hole nozzle.

2.2. Formulation of Optimization

The optimal design method using the metamodel defines the objective function and design parameters through the formulation of optimization. The objective function is a value representing performance and may be maximized or minimized according to the necessity of the optimization process. The values of the major design parameters are specified according to the factors which control the performance of the SCR system. In this optimization problem of SCR system performance, the UI value is selected as an objective function to maximize performance, and the definition of design parameters is mentioned in Table 2. The design parameter sets specify upper and lower ranges based on the initial value. The range of design parameters has been designated by a trial-and-error method so that it conserves the overall design drawings of the SCR system and prevents modeling errors.

Table 2. Boundary condition range for each parameter.

| No. | Major Design Parameters | Unit | Design Parameter Sets | | |
|-----|---|------|-----------------------|-------------|-------------|
| | | | Initial | Upper Limit | Lower Limit |
| 1 | A: Distance between the Urea Injector and Mixer | mm | 85 | 95 | 75 |
| 2 | B: Inflow Angle of the Exhaust Gas | deg. | 109 | 114 | 104 |
| 3 | C: Angle of the Urea Injector and Mixer | deg. | 110 | 115 | 105 |
| 4 | D: Mounting Angle of the Mixer | deg. | 0 | 10 | −10 |
| 5 | E: Number of Mixer Blades | No. | 6 | 8 | 4 |
| 6 | F: Bending Angle of Mixer Blades | deg. | 120 | 125 | 115 |
| 7 | G: Distance between the Mixer and SCR Cone | mm | 167 | 187 | 147 |
| 8 | H: Length of the SCR Cone | mm | 166 | 186 | 146 |

When the formalization is complete, performance optimization proceeds according to the process in Figure 2, which shows a flowchart of the SCR system optimization. The Formulation of optimization step comprises defining the design parameters as shown in Table 2 and defining an objective function. The Sampling step entails finding an experimental point for constructing the metamodel and uses multi-start local optimization

(MLO), query-by-commitment (QBC) using EDT, and multiple maximum distance sampling (MMDS) techniques developed by PIDOTECH [16]. In the next step, a model is designed with CATIA for the experimental points generated in the Sampling step, and numerical analysis is performed with STAR-CCM+ to obtain the UI value. In the Generate Metamodel step, a metamodel is generated from the obtained experimental points and numerical analysis results. Accuracy Convergence 1 is the process of verifying the accuracy of the metamodel by comparing the results of the test data between the predicted and actual numerical values.

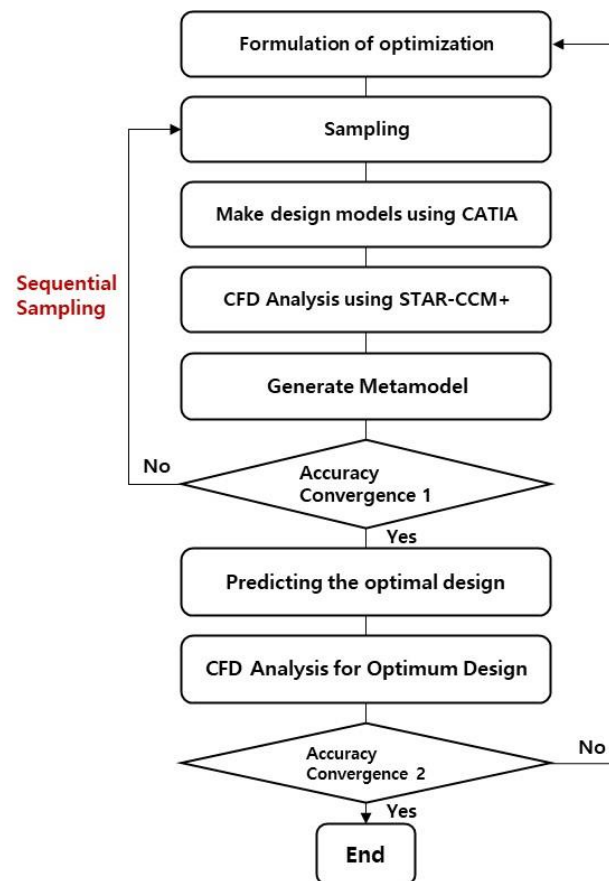


Figure 2. Flowchart of the optimization process using the metamodel.

The accuracy of the metamodel is calculated as a normalized root mean square error (Norm. RMSE) by comparing the prediction result with the actual result based on the metamodel generated for each iteration. Norm. RMSE is calculated using Equation (4) [32,33]. Maximum absolute error (Max. Abs. Error) is the largest value of the absolute errors and is calculated using Equation (5). When the verification of the metamodel is completed at Accuracy Convergence 1, it can predict the optimal design. The predicted results are calculated by computational fluid dynamics (CFD) under the same optimal design conditions. Finally, the accuracy is verified at Accuracy Convergence 2 using Equation (6). If the accuracy of the prediction results is low, the optimization process will proceed again after checking the problem in the Formulation of optimization step [13,34].

$$\text{Norm.RMSE} = \frac{\text{RMSE}}{Q_3 - Q_1} = \frac{\sqrt{\frac{1}{n_{\text{test}}} \sum (y - \hat{y})^2}}{Q_3 - Q_1} \quad (4)$$

$$\text{Max.Abs.Error} = \text{Max}[y_1 - \hat{y}_1, y_2 - \hat{y}_2, \dots, y_8 - \hat{y}_8] \quad (5)$$

$$\text{Maching Ratio}(\%) = \frac{y}{\hat{y}} \times 100 \quad (6)$$

where, n_{test} is the number of test points, y is the value of performance calculated by CFD, \hat{y} is the predicted value of performance through the metamodel, Q_3 is the 3rd quartile, and Q_1 is the 1st quartile. The metamodeling algorithm has been ranked by the PIA_{NO} tool and is equipped with various algorithms [20]. In this study, the Kriging, EDT, and RBF algorithms are selected. Kriging is a representative interpolation model and has excellent predictive performance in a data group with many design parameters and strong nonlinearity [35]. It also provides statistical estimates and does not depend on the user's experience because it optimizes parameters through the maximum likelihood estimation method (MLE) [36,37]. EDT refers to a method of generating multiple decision trees and predicting them as the average of each decision tree result [38,39]. It is known to improve predictability and performance mainly when dealing with large regression models [40]. The EDT model can be subclassified into tree bagging, random forest, and hybrid ensemble decision tree models [41,42]. RBF uses a kernel function suitable for each data set. It has the advantage of learning being nonlinear and fast [43,44]. Both the interpolation and regression models in RBF can be predicted and are divided into radial basis function interpolation (RBF_i) and radial basis function regression (RBF_r) [45,46].

3. Results of Optimization

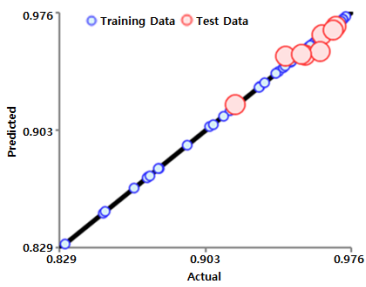
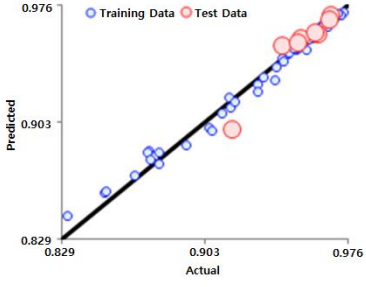
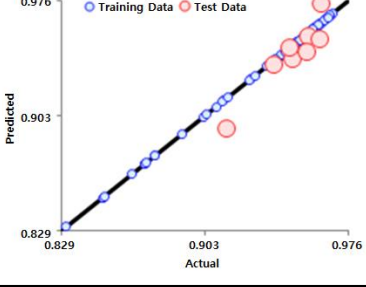
3.1. Optimization with the Metamodel

The results from the optimization process of the metamodeling are summarized in Table 3, and the detailed result is shown in Appendix A. In Appendix A, Table A1 shows the training data at the first iteration, Table A2 shows the training data at the second iteration, Table A3 shows the training data at the third iteration, Table A4 shows the training data at the fourth iteration, and Table A5 shows the test data. The plot mentioned in Table 3 is a graph of the accuracy of the metamodel, wherein the Y coordinate is the predicted result, and the X coordinate represents the actual numerical analysis value. The accuracy of the metamodel is higher as both the training (blue) and test (red) data match, and the results are shown in a linear graphical pattern. Numerically, Norm. RMSE from Equation (4) and Max. Abs. Error from Equation (5) are used to determine the accuracy of the metamodel [32].

Table 3 shows that the Norm. RMSE value of the RBF_i metamodel is 82.5%. As a result, it is confirmed that the prediction performance is poor among the three metamodels. The EDT metamodel (57.0%) at the Accuracy Convergence 1 step is better than the RBF_i metamodel result (82.5%). However, the error value is reduced in the EDT metamodel, but the maximum absolute error value is still 0.02, signifying an error rate of about 2%. Empirically, if an error value is of more than 1%, there exists a major issue because there is a large difference in the actual test results. Finally, the Kriging metamodel shows the lowest error rate (28.5%) among the three models. The maximum absolute error value is also 0.008, which is an error rate of less than 1%. Therefore, the optimization in this work is carried out by constructing a metamodel using the best-performing Kriging algorithm.

The performance optimization result using the Kriging metamodel is predicted as shown in Figure 3. The UI of the objective function is predicted to be 0.97461, which is 1.9% more than the predicted value (0.95641) of the initial design models. The convergence history and changes after the optimal design indicators show an increasing trend in the value of design parameters A, B, C, and G during the optimization process. The D and E design parameters changed the most as compared to the initial design parameters. The rate of change for the design parameters shown in Figure 3 is the ratio of the difference between the initial value and the optimal value with the initial value.

Table 3. Accuracy result of the metamodels.

| Ranking No. | Algorithm | Plot | Norm. RMSE(%) | RMSE | Max. Abs. Error |
|-------------|-----------|--|---------------|-------|-----------------|
| 1 | KRG |  | 28.5% | 0.004 | 0.008 |
| 2 | EDT |  | 57.0% | 0.008 | 0.020 |
| 3 | RBFi |  | 82.5% | 0.011 | 0.021 |

| Design Parameter | No. | Parameter | Convergence History | Changes after Optimal Design | Low Limit | Initial Value | Optimal Value | Rate of Change for Design Parameter | Upper Limit |
|--------------------|-----|----------------------------|---|------------------------------------|------------|---------------|---------------|---------------------------------------|------------------------|
| | 1 | A |  | Decrease | 75.00 | 85.00 | 80.42 | -5.4% | 95.00 |
| | 2 | B |  | Decrease | 104.00 | 109.00 | 107.38 | -1.5% | 114.00 |
| | 3 | C |  | Decrease | 105.00 | 110.00 | 108.02 | -1.8% | 115.00 |
| | 4 | D |  | Increase | -10.00 | 0.00 | 5.67 | 28.4% | 10.00 |
| | 5 | E |  | Increase (Close to Upper Limit) | 4.00 | 6.00 | 8.00 | 33.3% | 8.00 |
| | 6 | F |  | Increase | 115.00 | 120.00 | 121.21 | 1.0% | 125.00 |
| | 7 | G |  | Decrease | 147.00 | 167.00 | 163.97 | -1.8% | 187.00 |
| | 8 | H |  | Increase | 146.00 | 166.00 | 171.03 | 3.0% | 186.00 |
| Objective Function | No. | Name of Objective Function | Convergence History | Changes after Optimal Design | Importance | Initial Value | Optimal Value | Rate of Change for Objective Function | Maximum/Minimum/Target |
| | 1 | NH3_UI |  | Improvement | 1.00 | 0.95641 | 0.97461 | 1.9% | ↑ |

Figure 3. Result of optimization using the Kriging metamodel in the PIANO tool.

Table 4 shows the results which are compared between the prediction results and the CFD results of Accuracy Convergence 2 in Figure 2. CFD analysis is calculated using the same design parameters used for prediction. The performance-optimization prediction-result value is 0.97461, and the actual numerical analysis result is 0.97293. The matching rate is calculated by Equation (6) and is an indicator to determine the matching ability of both the predicted and actual CFD NH₃ UI values. It is confirmed that the predicted value

and the actual result match 99.83%. Therefore, the optimization prediction result using the metamodel can be applied with great confidence.

Table 4. Result of the CFD analysis compared to the metamodel optimization.

| No. | Major Design Parameters | Unit | Value | NH ₃ UI | |
|-------------------|---|------|--------|--------------------|---------|
| | | | | Prediction | CFD |
| 1 | A: Distance between the Urea Injector and Mixer | mm | 80.42 | | |
| 2 | B: Inflow Angle of the Exhaust Gas | deg. | 107.38 | | |
| 3 | C: Angle of the Urea Injector and Mixer | deg. | 108.02 | | |
| 4 | D: Mounting Angle of the Mixer | deg. | 5.67 | 0.97461 | 0.97293 |
| 5 | E: Number of Mixer Blades | No. | 8 | | |
| 6 | F: Bending Angle of Mixer Blades | deg. | 121.21 | | |
| 7 | G: Distance between the Mixer and SCR Cone | mm | 163.97 | | |
| 8 | H: Length of the SCR Cone | mm | 171.03 | | |
| Matching Rate (%) | | | | 99.83 | |

Table 5 shows the contribution of each design parameter numerically. It can classify objectively the importance of each design parameter. In the previous study [23], it was objectively impossible to analyze the design parameters as shown in Table 5. Consequently, there is a waste of time and cost because all of them were considered in the evaluation without classifying the design parameters that were less related to the performance improvement. Therefore, the results of the contribution analysis of Table 5 are very useful in defining the design parameters. Most design parameters except D, E, and F have contribution values of less than 10%. This means that there is no effect on performance improvement from other design parameters, namely A, B, C, G, and H. The number of blades of the mixer (E, 100%) absolutely contributed to the performance improvement, followed by the mixer blade angle (F, 22%), and the mixer rotation angle (D, 19%). This shows that the design parameters (D, E, and F) related to the mixer have significant contributions in improving the performance of the SCR system. The improvement of UI performance due to the optimization of the structural design parameters can also be confirmed by the experimental analysis carried out by Wardana et al. [5] and Jeong et al. [8]. Therefore, if optimization is focused on the design parameters of the mixer, it is estimated to be effective in reducing time and cost.

Table 5. Contribution analysis of the design parameters in the metamodel.

| No. | Major Design Parameters | Contribution Analysis [%] |
|-----|---|---------------------------|
| 1 | A: Distance between the Urea Injector and Mixer | 4 |
| 2 | B: Inflow Angle of the Exhaust Gas | 7 |
| 3 | C: Angle of the Urea Injector and Mixer | 0 |
| 4 | D: Mounting Angle of the Mixer | 19 |
| 5 | E: Number of Mixer Blades | 100 |
| 6 | F: Bending Angle of Mixer Blades | 22 |
| 7 | G: Distance between the Mixer and SCR Cone | 0 |
| 8 | H: Length of the SCR Cone | 3 |

3.2. Comparison of Results

Table 6 shows the results of the optimization of the base model using the DOE model and metamodel. In the three models, the design parameters G and H, related to the pipe length and SCR cone length, respectively, are changed in an increasing direction. In the case of G, the value for the base model is 147 mm, and it is increased to 187 mm during the DOE optimization and to 163.97 mm during the metamodel optimization. In the case of H, the value for the base model is 146 mm, and it is increased to 166 mm during the DOE optimization and 171.03 mm during the metamodel optimization. The bending angle of

the mixer blades (F) is changed in a decreasing direction. In the case of F, the value for the base model is 125 deg, and it is decreased to 115 deg during the DOE optimization and to 121.208 deg during the metamodel optimization. The UI compared with the base model (0.959639) is improved not only in the DOE optimization of previous studies (0.973499) [23] but also in the metamodel optimization of this work (0.972931). Therefore, both the DOE and metamodel optimization methods can improve UI performance. The results of the integrated analysis can be helpful to determine the design parameters.

Table 6. Design modeling of the base Model and DOE optimization and metamodel optimization.

| Base Model | DOE Optimization | Metamodel Optimization |
|------------------------------|------------------------------|------------------------------|
| | | |
| NH ₃ UI: 0.959639 | NH ₃ UI: 0.973499 | NH ₃ UI: 0.972931 |

In Table 7, the results of optimization, data quantity, contribution, and prediction are mentioned. They are compared with the results of previous studies [23] and are summarized in Table 7. The base model has been designed by evaluating only one dataset based on the experiment. Therefore, there are no data to compare the evaluation results, and the contribution analysis and prediction process cannot be evaluated. As the contribution and prediction results for base model and DOE optimization cannot be checked, the contribution and prediction results are marked as N/A. The upward arrow symbol shown in Table 7, indicates that the results of optimization for DOE optimization and metamodel optimization have improved compared to the base model by 1.44% and 1.38%, respectively.

Table 7. Summary of the base model, DOE optimization, and metamodel optimization.

| Classification | Base Model | DOE Optimization | Metamodel Optimization |
|-------------------------|------------|--------------------|------------------------|
| Results of Optimization | 0.959639 | 0.9734991 (1.44%↑) | 0.972931(1.38%↑) |
| Data Quantity | 1 | 27 | 87 |
| Contribution | N/A | N/A | E > F > D |
| Prediction | N/A | N/A | Predictable |

Moreover, the uniformity index and the NO_x purification efficiency can be correlated as shown in Equations (7)–(9):

$$\text{Final UI output} = 1 - \left(\frac{(0.5/19)}{\text{Average NO}_x \text{ purification efficiency} \times \text{Distribution sum of NO}_x \text{ purification efficiency}} \right) \quad (7)$$

$$\text{NO}_x \text{ purification efficiency} = \left(\frac{\text{Front} - \text{end NO}_x - \text{Back} - \text{end NO}_x}{\text{Front} - \text{end NO}_x} \right) \times 100 \quad (8)$$

$$\text{Distribution sum of NO}_x \text{ purification efficiency} = \sqrt{\sum_1^{19} (\text{Point NO}_x \text{ purification efficiency} - \text{Average NO}_x \text{ purification efficiency})^2} \quad (9)$$

The variables entered into each of Equations (7)–(9) are based on the engine operating point (EOP) defined by the user. In this study, the most common EOP conditions are used and are detailed in Appendix A Table A6. After calculating the front-end NO_x and the

back-end NO_x, it can be said that when the UI performance is relatively improved by 1.44% compared to the base model, the NO_x purification efficiency is improved by 30.95%. This indicates that with the optimization of design parameters and a minor increment in UI performance, there is a significant increase in NO_x purification efficiency.

In the previous work [23], optimization using the DOE method involved 27 experimental points generated through an orthogonal arrangement. The results were based on selecting the highest performance value from these points, making it challenging to ascertain contribution and prediction accuracy. The DOE method's uncertainty in the optimization results arises because it only covers a part of the design parameter range. However, in this study, metamodel optimization is employed, utilizing 87 data points generated through a sequential sampling method. The metamodel allows us to predict the maximum performance point across the entire range of design parameters. Sequential sampling ensures that only essential data are collected, making metamodel generation efficient and enabling accurate performance predictions. Additionally, the metamodel facilitates the analysis of design parameter contributions and performance value prediction. Effectively leveraging these advantages can significantly reduce time and cost by minimizing unnecessary numerical analysis and experiments. Although DOE and metamodel optimization are distinct methods, both exhibit an improved performance compared to the base model, offering promising approaches for enhancing the UI performance of the SCR system. In terms of analysis and result utilization, the metamodel method proves to be more effective than the DOE optimization and the base model.

4. Conclusions

In this study, various methods were explored for the structural optimization of the selective catalytic reduction system to maximize the uniformity index performance. Three algorithms, namely, ensemble decision tree, Kriging, and radial basis function were utilized to generate metamodels. The Kriging metamodel showed the lowest error compared to ensemble decision tree and radial basis function. The DOE method resulted in a 1.44% improvement in performance compared to the base model. Similarly, the metamodel method exhibited a performance enhancement of 1.38% over the base model. Since the metamodel analyzed the entire range of design parameters, the maximum uniformity index performance achieved in the present system is 0.973. By enhancing the uniformity index by 1.44% relative to the base model, there was a noteworthy 30.95% improvement in NO_x purification efficiency. This exhibits the crucial importance of optimizing the uniformity index performance through structural optimization. Thus, using the metamodel proves to be as accurate as the existing DOE method while also allowing for the analysis of design variable contributions, facilitating an efficient result analysis. In the future, the results of this study can be verified with test equipment, further validating the analysis model.

Author Contributions: Methodology, S.K., Y.P. and S.Y.; software, S.Y.; validation, Y.P. and S.Y.; formal analysis, S.K. and S.Y.; investigation, S.K.; resources, S.K., Y.P. and S.Y.; data curation, S.K. and Y.P.; writing—review and editing, S.L. and U.K.C.; funding acquisition, O.L. and W.C. All authors have read and agreed to the published version of the manuscript.

Funding: This work was supported by Regional Innovation Cluster Development (R&D) by the Ministry of Trade, Industry and Energy (MOTIE, Korea) [Project Name: Open Innovation Project for Convergence Industry of Battery/Fuel Cell for Mobility Electrification and Energy Production/Storage (P0025406)]. This result was supported by "Regional Innovation Strategy (RIS)" through the National Research Foundation of Korea (NRF) funded by the Ministry of Education (MOE) (2021RIS-003). This work was supported by Korea Institute of Planning and Evaluation for Technology in Food, Agriculture and Forestry (IPET) and Korea Smart Farm R&D Foundation (KosFarm) through Smart Farm Innovation Technology Development Program, funded by Ministry of Agriculture, Food and Rural Affairs (MAFRA) and Ministry of Science and ICT (MSIT), Rural Development Administration (RDA) (1545024470).

Institutional Review Board Statement: Not applicable.

Informed Consent Statement: Not applicable.

Data Availability Statement: Not applicable.

Acknowledgments: The authors appreciate the anonymous reviewers for their constructive comments and suggestions that significantly improved the quality of this manuscript.

Conflicts of Interest: The authors declare no conflict of interest.

Abbreviations

| | |
|-----------------|-------------------------------------|
| SCR | Selective Catalytic Reduction |
| UI | Uniformity Index |
| EDT | Ensemble Decision Tree |
| RBFi | Radial Basis Function Interpolation |
| RBFr | Radial Basis Function Regression |
| RMSE | Root Mean Square Error |
| Norm. RMSE | Normalized Root Mean Square Error |
| Max. Abs. Error | Maximum Absolute Error |
| DOE | Design of Experiments |
| MLO | Multi-start Local Optimization |
| QBC | Query-by-Commitment |
| MMDS | Multiple Maximum Distance Sampling |
| CFD | Computational Fluid Dynamics |
| MLE | Maximum Likelihood Estimation |

Appendix A

Table A1. 1st training data for the optimal creation of the metamodel.

| No. | A | B | C | D | E | F | G | H | NH3 UI |
|---------|----|-----|-----|-----|---|-----|-----|-----|--------|
| Case 1 | 95 | 114 | 115 | 10 | 8 | 125 | 187 | 186 | 0.964 |
| Case 2 | 95 | 114 | 115 | −10 | 4 | 115 | 187 | 146 | 0.833 |
| Case 3 | 95 | 109 | 110 | 10 | 8 | 125 | 167 | 166 | 0.966 |
| Case 4 | 95 | 109 | 110 | 0 | 6 | 120 | 167 | 146 | 0.943 |
| Case 5 | 95 | 109 | 110 | −10 | 4 | 115 | 167 | 186 | 0.867 |
| Case 6 | 95 | 104 | 105 | 0 | 6 | 120 | 147 | 186 | 0.962 |
| Case 7 | 85 | 109 | 105 | 0 | 4 | 125 | 187 | 166 | 0.851 |
| Case 8 | 85 | 109 | 105 | −10 | 8 | 120 | 187 | 146 | 0.963 |
| Case 9 | 85 | 104 | 115 | 10 | 6 | 115 | 167 | 166 | 0.955 |
| Case 10 | 85 | 104 | 115 | 0 | 4 | 125 | 167 | 146 | 0.853 |
| Case 11 | 85 | 104 | 115 | −10 | 8 | 120 | 167 | 186 | 0.970 |
| Case 12 | 85 | 114 | 110 | 10 | 6 | 115 | 147 | 146 | 0.951 |
| Case 13 | 85 | 114 | 110 | −10 | 8 | 120 | 147 | 166 | 0.964 |
| Case 14 | 75 | 104 | 110 | 10 | 4 | 120 | 187 | 186 | 0.874 |
| Case 15 | 75 | 104 | 110 | 0 | 8 | 115 | 187 | 166 | 0.973 |
| Case 16 | 75 | 104 | 110 | −10 | 6 | 125 | 187 | 146 | 0.943 |
| Case 17 | 75 | 114 | 105 | 0 | 8 | 115 | 167 | 146 | 0.966 |
| Case 18 | 75 | 114 | 105 | −10 | 6 | 125 | 167 | 186 | 0.956 |
| Case 19 | 75 | 109 | 115 | 0 | 8 | 115 | 147 | 186 | 0.968 |

Table A2. 2nd training data for the optimal creation of the metamodel.

| No. | A | B | C | D | E | F | G | H | NH3 UI |
|---------|-------|--------|--------|-------|---|--------|--------|--------|--------|
| Case 20 | 95 | 104 | 115 | 10 | 4 | 125 | 187 | 146 | 0.894 |
| Case 21 | 79.11 | 112.13 | 106.63 | 3.87 | 7 | 122.24 | 152.07 | 158.89 | 0.966 |
| Case 22 | 92.33 | 108.93 | 113.6 | −9.33 | 7 | 122.25 | 170.47 | 158 | 0.967 |
| Case 23 | 78.35 | 108.47 | 108.4 | −8.54 | 6 | 116.98 | 170.45 | 166.11 | 0.965 |
| Case 24 | 77.93 | 105.93 | 106.05 | 4 | 6 | 122.13 | 148.65 | 172.39 | 0.964 |
| Case 25 | 89.92 | 110.41 | 112.17 | 9.15 | 6 | 115.27 | 153.42 | 165.26 | 0.963 |
| Case 26 | 75 | 114 | 105 | 10 | 4 | 125 | 187 | 146 | 0.906 |
| Case 27 | 90.6 | 104.4 | 107.58 | 0.83 | 5 | 118.87 | 173.93 | 177.7 | 0.957 |
| Case 28 | 80.37 | 109.27 | 107.07 | −7.37 | 4 | 120.66 | 185.4 | 179.87 | 0.916 |
| Case 29 | 94.05 | 113.49 | 105.67 | −0.92 | 6 | 124.04 | 183.44 | 182.53 | 0.916 |
| Case 30 | 81.93 | 113.53 | 107.74 | −6.93 | 4 | 118.73 | 148.4 | 149.64 | 0.931 |
| Case 31 | 89.8 | 110.6 | 113.63 | 2.72 | 5 | 124.67 | 162.73 | 178.54 | 0.951 |
| Case 32 | 76.18 | 112.24 | 106.76 | −0.59 | 5 | 120.29 | 163.23 | 171.88 | 0.954 |
| Case 33 | 77.35 | 108.12 | 112.65 | 6.49 | 6 | 117.35 | 184.65 | 181.29 | 0.962 |
| Case 34 | 82.05 | 109.3 | 111.47 | 9.99 | 5 | 123.23 | 182.28 | 157.76 | 0.944 |
| Case 35 | 82.06 | 109.29 | 109.12 | −8.82 | 6 | 115 | 170.53 | 155.41 | 0.961 |
| Case 36 | 84.41 | 106.35 | 113.24 | 6.47 | 7 | 119.89 | 156.41 | 183.65 | 0.969 |
| Case 37 | 85.59 | 110.47 | 114.41 | 5.29 | 4 | 118.53 | 160.13 | 150.71 | 0.918 |
| Case 38 | 90.29 | 111.06 | 110.29 | 8.82 | 5 | 116.77 | 172.88 | 178.03 | 0.952 |
| Case 39 | 92.65 | 104.01 | 106.76 | −6.47 | 7 | 118.49 | 147.01 | 167.16 | 0.968 |

Table A3. 3rd training data for the optimal creation of the metamodel.

| No. | A | B | C | D | E | F | G | H | NH3 UI |
|---------|-------|--------|--------|-------|---|--------|--------|--------|--------|
| Case 40 | 75.00 | 107.13 | 109.38 | 6.25 | 8 | 121.31 | 174.50 | 171.00 | 0.975 |
| Case 41 | 84.33 | 104.33 | 111.84 | 7.47 | 7 | 121.10 | 170.19 | 180.83 | 0.970 |
| Case 42 | 94.00 | 111.83 | 110.93 | −7.88 | 8 | 118.33 | 160.34 | 183.84 | 0.973 |
| Case 43 | 87.66 | 109.34 | 112.34 | −1.44 | 6 | 116.43 | 184.86 | 172.18 | 0.961 |
| Case 44 | 93.54 | 112.13 | 114.74 | 5.95 | 5 | 124.45 | 165.67 | 160.41 | 0.947 |
| Case 45 | 87.32 | 110.40 | 106.93 | −4.01 | 7 | 121.29 | 174.20 | 185.27 | 0.971 |
| Case 46 | 78.24 | 105.72 | 111.10 | 6.62 | 7 | 120.40 | 164.60 | 153.32 | 0.966 |
| Case 47 | 81.87 | 105.79 | 106.20 | 2.93 | 7 | 117.65 | 185.81 | 171.87 | 0.970 |
| Case 48 | 93.98 | 110.13 | 112.46 | −2.90 | 8 | 119.14 | 181.93 | 152.67 | 0.968 |
| Case 49 | 76.49 | 107.40 | 107.80 | 4.20 | 7 | 118.87 | 155.80 | 181.46 | 0.973 |
| Case 50 | 92.45 | 110.15 | 105.30 | −8.39 | 5 | 124.13 | 149.92 | 176.13 | 0.959 |
| Case 51 | 79.66 | 104.73 | 112.55 | 10.00 | 4 | 124.67 | 155.59 | 174.99 | 0.939 |
| Case 52 | 85.92 | 109.93 | 110.61 | −0.67 | 5 | 115.93 | 149.56 | 172.15 | 0.958 |
| Case 53 | 94.73 | 107.80 | 106.27 | 1.41 | 4 | 121.33 | 147.74 | 150.81 | 0.930 |
| Case 54 | 94.73 | 107.33 | 105.50 | 2.02 | 6 | 116.87 | 159.27 | 154.05 | 0.960 |

Table A3. *Cont.*

| No. | A | B | C | D | E | F | G | H | NH3 UI |
|---------|-------|--------|--------|-------|---|--------|--------|--------|--------|
| Case 55 | 86.73 | 106.41 | 108.80 | −8.81 | 5 | 120.13 | 161.13 | 185.17 | 0.955 |
| Case 56 | 90.78 | 112.20 | 110.46 | 9.60 | 5 | 116.82 | 173.40 | 160.13 | 0.949 |
| Case 57 | 82.90 | 112.70 | 108.34 | 3.33 | 4 | 123.89 | 149.87 | 170.53 | 0.933 |
| Case 58 | 79.40 | 106.99 | 105.41 | 9.60 | 5 | 119.00 | 176.06 | 183.88 | 0.954 |
| Case 59 | 87.27 | 106.32 | 107.20 | 9.06 | 8 | 119.01 | 154.99 | 150.81 | 0.968 |

Table A4. 4th training data for the optimal creation of the metamodel.

| No. | A | B | C | D | E | F | G | H | NH3 UI |
|---------|-------|--------|--------|--------|---|--------|--------|--------|--------|
| Case 60 | 95.00 | 104.15 | 115.00 | −9.59 | 4 | 115.00 | 185.37 | 186.00 | 0.907 |
| Case 61 | 80.30 | 109.09 | 110.93 | 1.54 | 6 | 118.65 | 168.55 | 167.33 | 0.963 |
| Case 62 | 79.77 | 108.36 | 112.59 | −8.52 | 7 | 125.00 | 151.87 | 164.69 | 0.965 |
| Case 63 | 92.74 | 107.05 | 105.00 | −4.13 | 6 | 119.74 | 180.55 | 149.48 | 0.955 |
| Case 64 | 91.91 | 106.28 | 109.43 | −1.43 | 6 | 125.00 | 163.50 | 158.92 | 0.958 |
| Case 65 | 81.89 | 109.38 | 105.55 | 2.72 | 4 | 119.40 | 181.67 | 157.55 | 0.912 |
| Case 66 | 78.50 | 107.82 | 110.45 | −8.00 | 5 | 122.52 | 171.27 | 185.73 | 0.956 |
| Case 67 | 75.21 | 107.54 | 111.39 | 10.00 | 8 | 123.73 | 187.00 | 150.13 | 0.970 |
| Case 68 | 92.47 | 114.00 | 109.20 | 1.30 | 7 | 116.23 | 187.00 | 163.95 | 0.967 |
| Case 69 | 75.12 | 107.91 | 105.98 | 4.40 | 6 | 116.00 | 181.99 | 186.00 | 0.967 |
| Case 70 | 80.99 | 104.00 | 109.27 | 9.23 | 4 | 115.00 | 182.54 | 164.13 | 0.919 |
| Case 71 | 82.85 | 110.64 | 114.97 | 1.46 | 8 | 115.44 | 147.00 | 146.00 | 0.962 |
| Case 72 | 75.25 | 106.40 | 115.00 | −10.00 | 6 | 123.69 | 168.34 | 164.43 | 0.960 |
| Case 73 | 89.27 | 109.79 | 113.13 | −4.23 | 5 | 117.72 | 166.33 | 176.41 | 0.953 |
| Case 74 | 75.00 | 109.68 | 113.21 | 2.79 | 6 | 120.27 | 183.22 | 171.52 | 0.961 |
| Case 75 | 95.00 | 112.46 | 112.34 | 9.54 | 5 | 125.00 | 183.33 | 172.67 | 0.944 |
| Case 76 | 89.98 | 112.41 | 107.63 | −3.03 | 6 | 121.32 | 170.63 | 164.14 | 0.962 |
| Case 77 | 85.41 | 114.00 | 111.84 | 6.03 | 7 | 123.98 | 161.83 | 161.77 | 0.964 |
| Case 78 | 95.00 | 106.40 | 108.55 | −1.02 | 8 | 120.07 | 167.55 | 175.93 | 0.972 |
| Case 79 | 81.39 | 111.45 | 109.64 | −2.66 | 5 | 120.34 | 147.00 | 156.92 | 0.954 |

Table A5. Test data for the optimal creation of the metamodel.

| No. | A | B | C | D | E | F | G | H | NH3 UI |
|--------|----|-----|-----|-----|---|-----|-----|-----|--------|
| Case 1 | 95 | 114 | 115 | 0 | 6 | 120 | 187 | 166 | 0.941 |
| Case 2 | 95 | 104 | 105 | 10 | 8 | 125 | 147 | 146 | 0.960 |
| Case 3 | 95 | 104 | 105 | −10 | 4 | 115 | 147 | 166 | 0.880 |
| Case 4 | 85 | 109 | 105 | 10 | 6 | 115 | 187 | 186 | 0.950 |
| Case 5 | 85 | 114 | 110 | 0 | 4 | 125 | 147 | 186 | 0.880 |
| Case 6 | 75 | 114 | 105 | 10 | 4 | 120 | 167 | 166 | 0.874 |
| Case 7 | 75 | 109 | 115 | 10 | 4 | 120 | 147 | 146 | 0.875 |
| Case 8 | 75 | 109 | 115 | −10 | 6 | 125 | 147 | 166 | 0.956 |

Table A6. Boundary conditions of CFD.

| a. SCR System | | | |
|--|------------------------------------|-----------------------------------|------------------------|
| No. | Classification | Unit | Value |
| 1 | Shell Material | SUS | 436 L |
| 2 | Mass Flow of Exhaust Gas | kg/h | 316 |
| 3 | Exhaust Gas Temp. | Max, °C | 411 |
| 4 | Turbo Charger | Max, RPM | 203,000 |
| 5 | Engine RPM | RPM | 3000 |
| 6 | AdBlue | mg/s | 105 |
| 7 | Urea Injection | mg/Injection | 30.6 |
| 8 | Injection Duration | msec | 81.6 |
| 9 | Pressure of Exhaust Gas | kPa | 9.8 |
| b. Urea injector nozzle holes | | | |
| No. | Classification | Unit | Value |
| 1 | Number | No. | 3 |
| 2 | Hole Diameter | µm | 120 |
| 3 | Diameter at Hole Center Positions | mm | 1.9 |
| 4 | Circumferential Distribution | deg. | 120 |
| 5 | Static Mass Flow | kg/h | 3.2 |
| c. Injection initialization | | | |
| No. | Classification | Unit | Value |
| 1 | Equivalent Spray Type | Type | 3-Hole Full Cone Spray |
| 2 | Cone Angle | deg. | 7 |
| 3 | Spray Angle | deg. | 7 |
| 4 | Estimated Initial Droplet Velocity | m/s | 24 |
| 5 | Droplet Diameter, SMD | µm | 100 |
| d. Information of Mesh modeling | | | |
| No. | Classification | Value | No. |
| 1 | Analysis Tool | Star-CCM + V12.04 | 1 |
| 2 | Mesh Type | Polyhedral | 2 |
| 3 | Total Mesh Quantity | 1,041,308 | 3 |
| 4 | Base Mesh Size | 4 mm | 4 |
| 5 | Surface Mesh Size | 50~100% (Compared Base Mesh Size) | 5 |
| 6 | Number of Prism Layers | 3 | 6 |
| 7 | Prism Layer Thickness | 0.25 (Compared Base Thickness) | 7 |
| 8 | Fine Mesh | Surface: 25%, Prism: 12.5% | 8 |

References

- Zhang, Z.; Dong, R.; Tan, D.; Duan, L.; Jiang, F.; Yao, X.; Yang, D.; Hu, J.; Zhang, J.; Zhong, W.; et al. Effect of structural parameters on diesel particulate filter trapping performance of heavy-duty diesel engines based on grey correlation analysis. *Energy* **2023**, *271*, 127025. [\[CrossRef\]](#)
- Zhang, Z.; Dong, R.; Lan, G.; Yuan, T.; Tan, D. Diesel particulate filter regeneration mechanism of modern automobile engines and methods of reducing PM emissions: A review. *Environ. Sci. Pollut. Res.* **2023**, *30*, 39338–39376. [\[CrossRef\]](#) [\[PubMed\]](#)
- Kim, H.-S.; Kasipandi, S.; Kim, J.; Kang, S.-H.; Kim, J.-H.; Ryu, J.-H.; Bae, J.-W. Current Catalyst Technology of Selective Catalytic Reduction (SCR) for NO_x Removal in South Korea. *Catalysts* **2021**, *10*, 52. [\[CrossRef\]](#)

4. Kaźmierski, B.; Kapusta, J. The importance of individual spray properties in performance improvement of a urea-SCR system employing flash-boiling injection. *Appl. Energy* **2023**, *329*, 120217. [CrossRef]
5. Wardana, M.; Oh, K.; Lim, O. Investigation of Urea Uniformity with Different Types of Urea Injectors in an SCR System. *Catalysts* **2020**, *10*, 1269. [CrossRef]
6. Mehdi, G.; Zhou, S.; Zhu, Y.; Shah, A.H.; Chand, K. Numerical Investigation of SCR Mixer Design Optimization for Improved Performance. *Processes* **2019**, *7*, 168. [CrossRef]
7. Jiao, Y.; Zheng, Q. Urea Injection and Uniformity of Ammonia Distribution in SCR System of Diesel Engine. *Appl. Math. Nonlinear Sci.* **2020**, *5*, 129–142. [CrossRef]
8. Jeong, S.; Kim, H.; Kim, H.; Kwon, O.; Park, E.; Kang, J. Optimization of the Urea Injection Angle and Direction: Maximizing the Uniformity Index of a Selective Catalytic Reduction System. *Energies* **2020**, *14*, 157. [CrossRef]
9. Park, K.; Hong, C.H.; Oh, S.; Moon, S. Numerical Prediction on the Influence of Mixer on the Performance of Urea-SCR System. *World Acad. Sci. Eng. Technol. Int. J. Mech. Aerosp. Ind. Mechatron. Eng.* **2014**, *8*, 972–978. [CrossRef]
10. Ye, J.; Lv, J.; Tan, D.; Ai, Z.; Feng, Z. Numerical analysis on enhancing spray performance of SCR mixer device and heat transfer performance based on field synergy principle. *Processes* **2021**, *9*, 786. [CrossRef]
11. Antony, J. *Design of Experiments for Engineers and Scientists*; Elsevier: Amsterdam, The Netherlands, 2014. [CrossRef]
12. Hoang, P.H.; Phan, H.N.; Nguyen, D.T.; Paolacci, F. Kriging Metamodel-Based Seismic Fragility Analysis of Single-Bent Reinforced Concrete Highway Bridges. *Buildings* **2021**, *11*, 238. [CrossRef]
13. Kim, S.E.; Yoo, Y.M. Optimization of a Permanent Magnet Synchronous Motor for e-Mobility Using Metamodels. *Appl. Sci.* **2022**, *12*, 1625. [CrossRef]
14. You, Y.-M. Optimal Design of PMSM Based on Automated Finite Element Analysis and Metamodeling. *Energies* **2019**, *12*, 4673. [CrossRef]
15. Chung, I.B.; Lee, Y.B.; Choi, D.H. Global metamodeling using sequential and adaptive sampling with two criteria for global exploration and local exploitation. *Korean Soc. Mech. Eng.* **2020**, 170–175.
16. Shin, Y.S.; Lee, Y.B.; Ryu, J.S.; Choi, D.H. Sequential approximate optimization using kriging metamodels. *Korean Soc. Mech. Eng.* **2005**, *29*, 1199–1208. [CrossRef]
17. Woo, S.H.; Ha, Y.C.; Yoo, J.W.; Josa, E.; Shin, D.H. Chassis Design Target Setting for a High-Performance Car Using a Virtual Prototype. *Appl. Sci.* **2023**, *13*, 844. [CrossRef]
18. You, Y.M. Multi-Objective Optimal Design of Permanent Magnet Synchronous Motor for Electric Vehicle Based on Deep Learning. *Appl. Sci.* **2020**, *10*, 482. [CrossRef]
19. Woldemariam, E.T.; Lemu, H.G.; Wang, G.A. CFD-Driven Valve Shape Optimization for Performance Improvement of a Micro Cross-Flow Turbine. *Energies* **2018**, *11*, 248. [CrossRef]
20. Introduction of PIAO. Available online: <http://www.pidotech.com> (accessed on 1 April 2018).
21. Park, H.R.; Jung, S.J. Design and Automated Optimization of an Internal Turret Mooring System in the Frequency and Time Domain. *J. Mar. Sci. Eng.* **2021**, *9*, 581. [CrossRef]
22. Chai, W.; Lipo, T.; Kwon, B.I. Design and Optimization of a Novel Wound Field Synchronous Machine for Torque Performance Enhancement. *Energies* **2018**, *11*, 2111. [CrossRef]
23. Kim, S.H.; Park, Y.J.; Yoo, S.B.; Lim, O.T. Development of Machine Learning Algorithms for Application in Major Performance Enhancement in the Selective Catalytic Reduction (SCR) System. *Sustainability* **2023**, *15*, 7077. [CrossRef]
24. Busca, G.; Lietti, L.; Ramis, G.; Berti, F. Chemical and mechanistic aspects of the selective catalytic reduction of NO_x by ammonia over oxide catalysts: A review. *Appl. Catal. B Environ.* **1998**, *18*, 1–36. [CrossRef]
25. Napolitano, P.; Liotta, L.F.; Guido, C.; Tornatore, C.; Pantaleo, G.; La Parola, V.; Beatrice, C. Insights of selective catalytic reduction technology for nitrogen oxides control in marine engine applications. *Catalysts* **2022**, *12*, 1191. [CrossRef]
26. Yim, S.D.; Kim, S.J.; Baik, J.H.; Nam, I.S.; Mok, Y.S.; Lee, J.H.; Cho, B.K.; Oh, S.H. Decomposition of urea into NH₃ for the SCR process. *Ind. Eng. Chem. Res.* **2004**, *43*, 4856–4863. [CrossRef]
27. Sorrels, J.L.; Randall, D.D.; Schaffner, K.S.; Fry, C.R. Selective catalytic reduction. In *EPA Air Pollution Control Cost Manual*; US Environmental Protection Agency Research Triangle Park: Durham, NC, USA, 2019; p. 7.
28. Tian, X.; Xiao, Y.; Zhou, P.; Zhang, W.; Chu, Z.; Zheng, W. Study on the mixing performance of static mixers in selective catalytic reduction (SCR) systems. *J. Mar. Eng. Technol.* **2015**, *14*, 57–60. [CrossRef]
29. Savci, I.H.; Gul, M.Z. A methodology to assess mixer performance for selective catalyst reduction application in hot air gas burner. *Alex. Eng. J.* **2022**, *61*, 6621–6633. [CrossRef]
30. Rogóż, R.; Kapusta, Ł.J.; Bachanek, J.; Vankan, J.; Teodorczyk, A. Improved urea-water solution spray model for simulations of selective catalytic reduction systems. *Renew. Sustain. Energy Rev.* **2020**, *120*, 109616. [CrossRef]
31. Zhu, Y.; Zhou, W.; Xia, C.; Hou, Q. Application and development of selective catalytic reduction technology for marine low-speed diesel engine: Trade-off among high sulfur fuel, high thermal efficiency, and low pollution emission. *Atmosphere* **2022**, *13*, 731. [CrossRef]
32. Shcherbakov, M.V.; Brebels, A.; Shcherbakova, N.L.; Tyukov, A.P.; Janovsky, T.A.; Kamaev, V.A.E. A Survey of Forecast Error Measures. *World Appl. Sci. J.* **2013**, *24*, 171–176.

33. Lin, Y.; Krishnapur, K.; Allen, J.K.; Mistree, F. Robust design: Goal formulations and a comparison of metamodeling methods. In Proceedings of the International Design Engineering Technical Conferences and Computers and Information in Engineering Conference, Las Vegas, NV, USA, 12–16 September 1999; American Society of Mechanical Engineers: New York, NY, USA, 1999; Volume 19715, pp. 1355–1367.
34. Ko, J.S.; Huh, J.H.; Kim, J.C. Overview of maximum power point tracking methods for PV system in micro grid. *Electronics* **2020**, *9*, 816. [[CrossRef](#)]
35. Qin, S.; Zhang, Y.; Zhou, Y.L.; Kang, J. Dynamic model updating for bridge structures using the kriging model and PSO algorithm ensemble with higher vibration modes. *Sensors* **2018**, *18*, 1879. [[CrossRef](#)] [[PubMed](#)]
36. Iapteff, L.; Jacques, J.; Rolland, M.; Celse, B. Reducing the number of experiments required for modelling the hydrocracking process with kriging through Bayesian transfer learning. *J. R. Stat. Soc. Ser. C Appl. Stat.* **2021**, *70*, 1344–1364. [[CrossRef](#)]
37. Yang, X.; Guo, X.; Ouyang, H.; Li, D. A Kriging model based finite element model updating method for damage detection. *Appl. Sci.* **2017**, *7*, 1039. [[CrossRef](#)]
38. Che, D.; Liu, Q.; Rasheed, K.; Tao, X. Decision tree and ensemble learning algorithms with their applications in bioinformatics. *Softw. Tools Algorithms Biol. Syst.* **2011**, *696*, 191–199. [[CrossRef](#)]
39. Pal, M. Ensemble learning with decision tree for remote sensing classification. *World Acad. Sci. Eng. Technol.* **2007**, *36*, 258–260. [[CrossRef](#)]
40. Bekdaş, G.; Cakiroglu, C.; Islam, K.; Kim, S.; Geem, Z.W. Optimum Design of Cylindrical Walls Using Ensemble Learning Methods. *Appl. Sci.* **2022**, *12*, 2165. [[CrossRef](#)]
41. Zhou, Z.H.; Tang, W. Selective ensemble of decision trees. In Proceedings of the Rough Sets, Fuzzy Sets, Data Mining, and Granular Computing: 9th International Conference, RSFDGrC 2003, Chongqing, China, 26–29 May 2003; Springer: Berlin/Heidelberg, Germany, 2003; pp. 476–483.
42. Ly, H.B.; Monteiro, E.; Le, T.T.; Le, V.M.; Dal, M.; Regnier, G.; Pham, B.T. Prediction and sensitivity analysis of bubble dissolution time in 3D selective laser sintering using ensemble decision trees. *Materials* **2019**, *12*, 1544. [[CrossRef](#)]
43. Buhmann, M.D. Radial basis functions. *Acta Numer.* **2000**, *9*, 1–38. [[CrossRef](#)]
44. Kalita, K.; Chakraborty, S.; Madhu, S.; Ramachandran, M.; Gao, X.Z. Performance analysis of radial basis function metamodels for predictive modelling of laminated composites. *Materials* **2021**, *14*, 3306. [[CrossRef](#)]
45. Havinga, J.; van den Boogaard, A.H.; Klaseboer, G. Sequential improvement for robust optimization using an uncertainty measure for radial basis functions. *Struct. Multidiscip. Optim.* **2017**, *55*, 1345–1363. [[CrossRef](#)]
46. Urquhart, M.; Ljungskog, E.; Sebben, S. Surrogate-based optimisation using adaptively scaled radial basis functions. *Appl. Soft Comput.* **2020**, *88*, 106050. [[CrossRef](#)]

Disclaimer/Publisher’s Note: The statements, opinions and data contained in all publications are solely those of the individual author(s) and contributor(s) and not of MDPI and/or the editor(s). MDPI and/or the editor(s) disclaim responsibility for any injury to people or property resulting from any ideas, methods, instructions or products referred to in the content.